

**Phase-field study of stress-induced polarization switching for
vibration energy harvesting: material influence**

Wang, D., Wang, L., and Melnik, R.

**Proceedings of SMART- 2017 (Eds.: A. Guemes et al), June 5-8, 2017,
Madrid, CIMNE Publisher, pp. 666-673,
ISBN: 978-84-946909-3-8, 2017.**

PHASE FIELD STUDY OF STRESS-INDUCED POLARIZATION SWITCHING FOR VIBRATION ENERGY HARVESTING: MATERIAL INFLUENCE

DAN WANG ^{*†}, LINXIANG WANG ^{*} AND RODERICK MELNIK [†]

^{*} State Key Laboratory of Fluid Power and Mechatronic Systems
Zhejiang University, Hangzhou, 310027, China

[†] MS2Discovery Interdisciplinary Research Institute
Wilfrid Laurier University, Waterloo, ON N2L 3L5, Canada
email: rmelnik@wlu.ca

Key words: Vibration Energy Harvesting, Material Influence, Phenomenological Thermodynamic Analysis, Phase Field Model.

Abstract. Recently, a novel method for vibration energy harvesting has been proposed, which is based on stress-induced polarization switching. A huge improvement in the energy output associated with this new method has been theoretically demonstrated. In the current paper, the influence of different materials on the energy harvesting performance is studied. Firstly, a phenomenological thermodynamic analysis based on a Landau-type elastic Gibbs energy is carried out, which gives a guidance for further investigations. Then, the state-of-the-art phase field model is implemented to study the hysteretic nonlinear phenomena involved in the energy harvesting process. The influence of different materials is carefully compared and discussed. Furthermore, the combined effects of the bias electric potential and bias resistance in different materials are presented and discussed in the context of future real implementations.

1 INTRODUCTION

In the past two decades, vibration energy harvesting has emerged as a promising method to power wireless sensor networks and implantable biomedical devices, generating great interest from researchers around the world [1-3]. Generally, there are three principal ways to convert the ambient vibrational energy into useful electricity---through electromagnetic, electrostatic and piezoelectric effects [4-6]. However, the energy density harvested via these three traditional approaches is still not sufficient, especially for applications in low-frequency vibrational environments. Different methods have been proposed in the literature to improve the energy harvesting performance, including but not limited to designing different mechanical structures to lower the natural frequency of the systems to meet the frequency range of the vibration sources , introducing nonlinear effects into the energy harvesting structures to broaden the resonate frequency range, and employing materials with better properties, e.g., using single-crystal ferroelectric materials in piezoelectric vibration energy harvesting, which has a supreme piezoelectric coefficient over commonly-used ceramics[7-9].

In addition, several innovative physics-based methods have also been proposed, such as those based on triboelectric nanogenerators [10, 11].

Recently, a new method has been proposed, which is based on stress-induced polarization switching phenomena in ferroelectric materials [12, 13]. Different from the traditional piezoelectric vibration energy harvesting, which is confined to the linear piezoelectric region, a non-180° ferroelastic polarization switching is induced in this new method to seek more polarization variations. The huge polarization changes associated with stress-induced polarization switching process result in a great improvement of the energy output. The energy density, which is several orders of magnitude higher than its counterpart harvested by traditional linear piezoelectric effect, has been theoretically demonstrated. In Ref. [13], by introducing a bias electric field, the robustness deficiency problem associated with the original prototype has been successfully tackled. Due to its great potential in real applications and the complicated nonlinear hysteretic phenomena involved, this new method requires a more detailed analysis.

In the current paper, the influence of different materials on the energy harvesting performance is under investigation. The differences between single crystal BaTiO₃ and PbTiO₃ ferroelectrics are carefully studied and discussed. Firstly, a phenomenological thermodynamic analysis based on a Landau-type elastic Gibbs energy is carried out, which gives a basic understanding of the differences between these two single crystals and their effects on the energy harvesting performance. Secondly, the energy harvesting process is studied via the state-of-the-art phase field model. The phase field simulations confirm the predictions from the thermodynamic analysis. Furthermore, the combined effects of the bias resistance and bias electric potential on the energy harvesting performance in these two cases are presented and discussed.

2 PHENOMENOLOGICAL THERMODYNAMIC ANALYSIS

To analyze the influence of different materials on the energy harvesting performance, BaTiO₃ and PbTiO₃ ferroelectric single crystals are considered. Firstly, a phenomenological thermodynamic analysis is carried out, which is based on a Landau-type elastic Gibbs energy that can be given as follows:

$$G(\mathbf{P}, \boldsymbol{\sigma}) = a_1(P_1^2 + P_2^2 + P_3^2) + a_{11}(P_1^4 + P_2^4 + P_3^4) + a_{12}(P_1^2 P_2^2 + P_1^2 P_3^2 + P_2^2 P_3^2) + a_{111}(P_1^6 + P_2^6 + P_3^6) + a_{112}[P_1^4(P_2^2 + P_3^2) + P_2^4(P_1^2 + P_3^2) + P_3^4(P_1^2 + P_2^2)] + a_{123}P_1^2 P_2^2 P_3^2 - \frac{1}{2}s_{11}(\sigma_{11}^2 + \sigma_{22}^2 + \sigma_{33}^2) - s_{12}(\sigma_{11}\sigma_{22} + \sigma_{11}\sigma_{33} + \sigma_{22}\sigma_{33}) - \frac{1}{2}s_{44}(\sigma_{12}^2 + \sigma_{13}^2 + \sigma_{23}^2) - Q_{11}(\sigma_{11}P_1^2 + \sigma_{22}P_2^2 + \sigma_{33}P_3^2) - Q_{12}[\sigma_{11}(P_2^2 + P_3^2) + \sigma_{22}(P_1^2 + P_3^2) + \sigma_{33}(P_1^2 + P_2^2)] - Q_{44}(\sigma_{12}P_1P_2 + \sigma_{13}P_1P_3 + \sigma_{23}P_2P_3). \quad (1)$$

The associated material parameters, taken from Ref. [14] (for temperature 25°C), are listed in Table 1. The contour plots of the two-dimensional free energy without external stress are presented in Figure 1. The spontaneous polarizations of the materials can be deduced by minimizing the elastic Gibbs energy with zero stress. The corresponding values for BaTiO₃ and PbTiO₃ are 0.27C/m² and 0.757C/m², respectively. Therefore, it is reasonable to expect that the output electric current of PbTiO₃ is approximately 3 times larger than that of BaTiO₃, as long as complete stress-induced polarization switching is induced at the same rate in both materials ($I = \frac{dQ}{dt}$, $Q \propto P$). With the same external resistance, the energy output will be about

9 times larger ($W = I^2Rt$). On the other side, the critical input stress, which is required to complete a ferroelastic polarization switching, is also very important in real applications. To give an approximation, a strategy based on the energy barrier theory is adopted:

$$\sigma_c = G_{\text{barrier}} / \varepsilon_{\text{diff}}^0, \quad (2)$$

where G_{barrier} is the energy barrier between states before and after the stress-induced polarization switching process. It can be approximated by the energy difference between the saddle point and the minimum point (as shown in Figure 1); $\varepsilon_{\text{diff}}^0$ is the associated spontaneous strain change during the polarization switching process, which equals to the longitudinal spontaneous strain ε_{11}^0 minus the transvers spontaneous strain ε_{22}^0 .

With simple calculations, the critical values required to induce polarization switching for BaTiO₃ and PbTiO₃ are 35.4 MPa and 625.6 MPa respectively, which means, approximately, a 20 times larger stress is required for PbTiO₃. In addition to the critical stress, several other important material-specific results are also provided, as listed in Table 2. It is noticed that the energy barrier for PbTiO₃ is more than 100 times larger than that for BaTiO₃, which can be used to estimate the inherent energy dissipation during the polarization switching process. Considering the fact that the energy output is only about 9 times larger, the energy efficiency of PbTiO₃ suffers. In conclusion, PbTiO₃ can give a larger energy output but requires a significantly larger critical stress. The choice of the material depends on application condition. For example, when a strong enough stress can be assessed and the energy density is the prime target, PbTiO₃ is always the first choice. It needs to be pointed out that the exact value obtained here is served only as an estimation. No bias electric field is taken into consideration, and the influence of domain walls or material defects are not considered either. Furthermore, the polarization switching phenomenon involved in this method is intrinsically nonlinear and hysteretic. Instead of a simple homogeneous switching, very complicated stress and electric field states can be present. Thus a more robust and detailed investigation is needed.

Table 1: Material parameters for the elastic Gibbs energy

Material parameters	a ₁	a ₁₁	a ₁₂	a ₁₁₁	a ₁₁₂	a ₁₂₃
BaTiO ₃	-2.8e7	-5.4e8	4.9e8	6.6e9	2.9e9	3.7e10
PbTiO ₃	-1.7e8	-7.3e7	7.5e8	2.6e8	6.1e8	-3.7e9
Material parameters	Q ₁₁	Q ₁₂	Q ₄₄	S ₁₁	S ₁₂	S ₄₄
BaTiO ₃	0.11	-0.043	0.059	8.3e-12	-2.7e-12	9.24e-12
PbTiO ₃	0.089	-0.026	0.0675	8e-12	-2.5e-12	9e-12

Table 2: Some important material-specific calculated results

	Spontaneous polarization P_0	Spontaneous strain (longitudinal) ϵ_{11}^0	Spontaneous strain (transverse) ϵ_{22}^0	Spontaneous strain change ϵ_{diff}^0
BaTiO ₃	0.27	0.0074	-0.0029	0.0103
PbTiO ₃	0.757	0.051	-0.015	0.066
	Energy barrier I $G_{barrier}$	Critical stress σ_c	Energy barrier II $G'_{barrier}^*$	Critical electric field E_c^{**}
BaTiO ₃	3.65e5	3.54e7	2.36e6	4.53e6
PbTiO ₃	4.12e7	6.256e8	7.39e7	4.88e7

*Energy barrier II is the energy barrier involved in 180° ferroelectric polarization switching, which can be approximated by the energy difference between the local maximum and minimum points.

**Critical electric field is an important constant in capturing 180° ferroelectric polarization switching phenomenon, which can be approximated by using the energy barrier II through the relation: $E_c = G'_{barrier}/(2 \cdot P_0)$

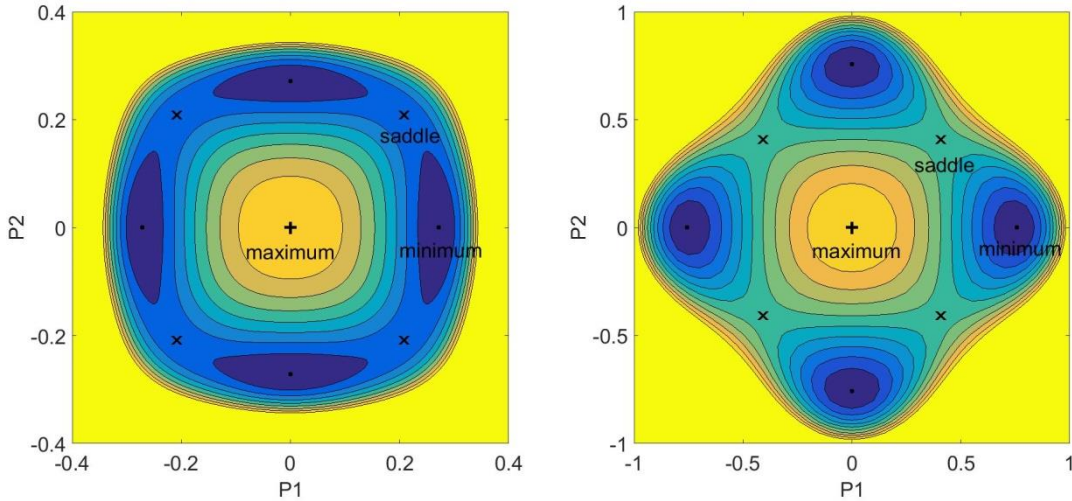


Figure 1: Contour plots of the two-dimensional free energy without external stress: (a) for BaTiO₃; (b) for PbTiO₃.

3 PHASE FIELD STUDY AND DISCUSSION

To further analyze the influence of materials, the state-of-the-art phase field model is implemented to study the energy harvesting process. The governing equation can be obtained as the gradient flow associated with the potential energy based on the Landau theory:

$$\mu \dot{P}_i = \left(\frac{\partial \Psi}{\partial P_{i,j}} \right)_{,j} - \frac{\partial \Psi}{\partial P_i} - \varphi_{,i}. \quad (3)$$

Here, $1/\mu > 0$ is the mobility; φ denotes the electric potential and Ψ is the potential energy in the following form:

$$\Psi(\nabla \mathbf{P}, \mathbf{P}, \boldsymbol{\varepsilon}) = \alpha_0(P_{1,1}^2 + P_{1,2}^2 + P_{1,3}^2 + P_{2,1}^2 + P_{2,2}^2 + P_{2,3}^2 + P_{3,1}^2 + P_{3,2}^2 + P_{3,3}^2) + \tilde{G}(\mathbf{P}, \boldsymbol{\varepsilon}), \quad (4)$$

where

$$\begin{aligned}\tilde{G}(\mathbf{P}, \boldsymbol{\varepsilon}) = & \alpha_1(P_1^2 + P_2^2 + P_3^2) + \alpha_{11}(P_1^4 + P_2^4 + P_3^4) + \alpha_{12}(P_1^2 P_2^2 + P_1^2 P_3^2 + P_2^2 P_3^2) + \\ & \alpha_{111}(P_1^6 + P_2^6 + P_3^6) + \alpha_{112}[P_1^4(P_2^2 + P_3^2) + P_2^4(P_1^2 + P_3^2) + P_3^4(P_1^2 + P_2^2)] + \\ & \alpha_{123}P_1^2 P_2^2 P_3^2 + \frac{1}{2}C_{11}(\varepsilon_{11}^2 + \varepsilon_{22}^2 + \varepsilon_{33}^2) + C_{12}(\varepsilon_{11}\varepsilon_{22} + \varepsilon_{11}\varepsilon_{33} + \varepsilon_{22}\varepsilon_{33}) + 2C_{44}(\varepsilon_{12}^2 + \varepsilon_{13}^2 + \\ & \varepsilon_{23}^2) - q_{11}(\varepsilon_{11}P_1^2 + \varepsilon_{22}P_2^2 + \varepsilon_{33}P_3^2) - q_{12}[\varepsilon_{11}(P_2^2 + P_3^2) + \varepsilon_{22}(P_1^2 + P_3^2) + \varepsilon_{33}(P_1^2 + P_2^2)] - \\ & 2q_{44}(\varepsilon_{12}P_1P_2 + \varepsilon_{13}P_1P_3 + \varepsilon_{23}P_2P_3).\end{aligned}\quad (5)$$

The expression for $\tilde{G}(\mathbf{P}, \boldsymbol{\varepsilon})$ is derived following the Legendre transformation of the elastic Gibbs energy $G(\mathbf{P}, \boldsymbol{\sigma})$. It needs to be pointed out that in the literature some misconceptions exist about the coefficients in the free energy. In Ref. [15, 16], the authors stated that the Landau coefficients were taken directly from Ref. [14]. However, it is noticed that the coefficients in Ref. [14] are for the elastic Gibbs free energy, rather than for the free energy used in the phase field model. Thus, a Legendre transformation is necessary. That is why the simulated normalized spontaneous polarization shown in Ref. [15] is around 1.5. The material parameters after the Legendre transformation are listed in Table 3. The gradient energy coefficient α_0 , taken in the current simulations for BaTiO₃ and PbTiO₃, is 2.8×10^{-10} Vm³/C and 1×10^{-10} Vm³/C respectively. The corresponding characteristic length scales ($l_0 = \sqrt{\alpha_0 P_0^2 / E_{\text{Barrier}}}$, which can be used as an approximation for the domain wall thickness) are 4.3nm and 2.0nm. In the simulation, the governing equation (3) is solved together with the elasticity and Maxwell equations. For simplicity, the simulations have been carried out for a two dimensional case. The computational domain is 160nm×20nm for both cases. The boundary conditions taken in the current simulations are the same as those used in Ref. [13]. The resulting model has been numerically implemented and solved in Comsol Multiphysics [17].

Firstly, simulations without external bias electric potential and resistance have been carried out to determine the critical stress value that is required to complete the stress-induced polarization switching process. The results for BaTiO₃ and PbTiO₃ are 32Mpa and 514Mpa respectively, which are consistent with the predictions from the energy barrier theory, as listed in Table 2. Further, some additional simulations have been carried out to determine the critical bias electric potential values for 180° ferroelectric switching. The results are 0.029V and 0.21V, respectively, for BaTiO₃ and PbTiO₃. The corresponding electric field values are 1.45MV/m and 10.5MV/m, which are approximately one fourth of the predicted values listed in Table 2.

Next, a series of simulations with different bias electric fields and different bias resistances have been carried out to investigate their combined effects. The external stress amplitudes for BaTiO₃ and PbTiO₃ in the simulations are 48Mpa and 740Mpa respectively, which are 1.25 times of the critical values for ferroelastic switching. The bias electric potential values are around one half of the critical values for 180° ferroelectric switching. To present combined effects, the bias resistance range has been determined based on numerical experiments.

The simulated results are shown in Figure 2 and Figure 3. With a constant bias electric potential, the energy output increases first, reaches its peak and then decreases, as the bias resistance increases. This behavior is observed in both cases. Further, we note that the energy peak will be improved when the bias electric potential increases, so will the associated bias resistance values. However, it does not mean that we can increase the bias electric potential without limit to improve the energy output. The material will break down with extreme electric fields and excessive stress. The peak energy output in the current simulations for

PbTiO_3 is approximately 100 times bigger than that for BaTiO_3 , which is different from the thermodynamic prediction. This can be explained by the fact that the optimized bias resistance values are used here. Instead, in the above thermodynamic analysis, the same resistance value is assumed. It needs to be pointed out the unit for the bias resistance in the results is the parameter μ instead of a real value. Moreover, for different materials, the parameter μ will be different. Indeed, the parameter μ is related to the relaxation phenomena and frequency-dependent properties in ferroelectric materials. We will address this issue in a separate publication. In addition, it is also noticed that, there is no big difference between the energy efficiency for both materials, which is around 30%. As pointed out, the internal energy dissipation is about 100 times bigger for PbTiO_3 . With a similar relationship in the energy output, it is reasonable to produce similar energy efficiency.

4 CONCLUSIONSS

In the current paper, the influence of different materials on the energy harvesting performance of a new method based on stress-induced polarization switching, has been carefully investigated. Firstly, a phenomenological thermodynamic analysis has been carried out, which has provided a primary guidance for further investigations. Then, the state-of-the-art phase field model has been implemented to analyze the energy harvesting processes and the involved hysteretic nonlinear phenomena. Finally, the combined effects of bias electric potential and bias resistance in both materials have been demonstrated and discussed in detail in the context of potential applications.

ACKNOWLEDGEMENTS

This work has been supported by the National Natural Science Foundation of China (Grant No. 51575478 and Grant No. 61571007). DW acknowledges the financial support from Zhejiang University for his visit to Wilfrid Laurier University. RM acknowledges the support from the NSERC and CRC program.

Table 3: Updated parameters for the phase field model

Updated parameters	α_1	α_{11}	α_{12}	α_{111}	α_{112}	α_{123}
BaTiO_3	-2.8e7	1.9e8	1.5e7	6.6e9	2.9e9	3.7e10
PbTiO_3	-1.7e8	4.2e8	7.3e8	2.6e8	6.1e8	-3.7e9
Updated parameters	q_{11}	q_{12}	q_{44}	c_{11}	c_{12}	c_{44}
BaTiO_3	1.3e10	-9.7e8	3.2e9	1.3e11	4.4e10	2.7e10
PbTiO_3	1.1e10	2.5e8	3.8e9	1.4e11	4.3e10	2.8e10

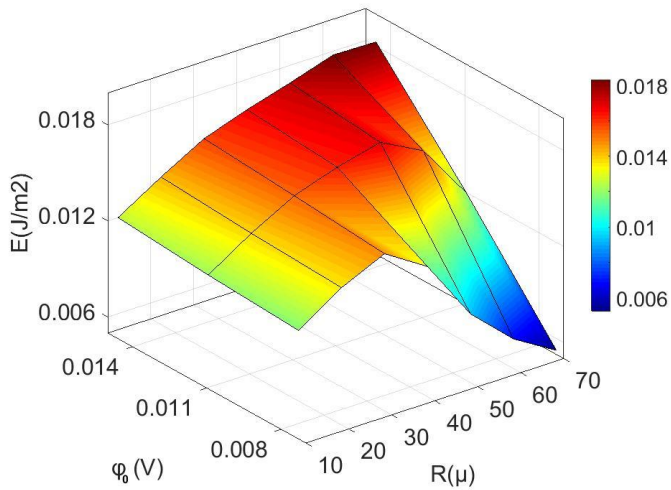


Figure 2: Energy output with respect to bias electric potential and bias resistance for BaTiO_3 .

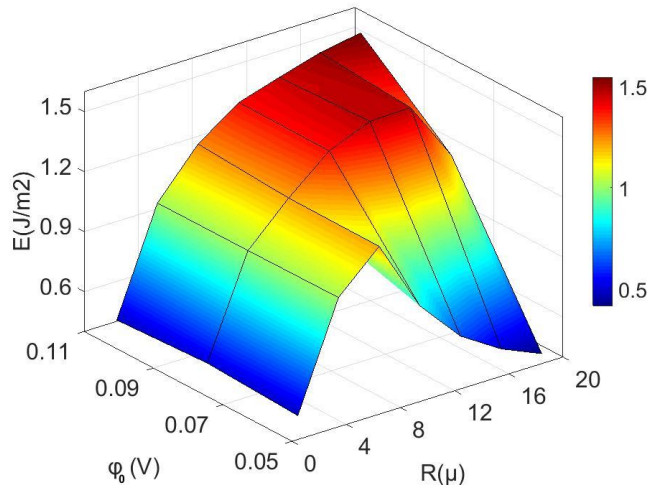


Figure 3: Energy output with respect to bias electric potential and bias resistance for PbTiO_3 .

REFERENCES

- [1] Shaikh, F. K., & Zeadally, S. (2016). Energy harvesting in wireless sensor networks: A comprehensive review. *Renewable and Sustainable Energy Reviews*, 55, 1041-1054.
- [2] Babayo, A. A., Anisi, M. H., & Ali, I. (2017). A Review on energy management schemes in energy harvesting wireless sensor networks. *Renewable and Sustainable Energy Reviews*, 76, 1176-1184.
- [3] Amin Karami, M., & Inman, D. J. (2012). Powering pacemakers from heartbeat vibrations using linear and nonlinear energy harvesters. *Applied Physics Letters*, 100(4), 042901.
- [4] Roundy, S., Wright, P. K., & Rabaey, J. (2003). A study of low level vibrations as a power source for wireless sensor nodes. *Computer communications*, 26(11), 1131-1144.
- [5] Invernizzi, F., Dulio, S., Patrini, M., Guizzetti, G., & Mustarelli, P. (2016). Energy

- harvesting from human motion: materials and techniques. *Chemical Society Reviews*, 45(20), 5455-5473.
- [6] Wang, W., Cao, J., Zhang, N., Lin, J., & Liao, W. H. (2017). Magnetic-spring based energy harvesting from human motions: Design, modeling and experiments. *Energy Conversion and Management*, 132, 189-197.
 - [7] Li, H., Tian, C., & Deng, Z. D. (2014). Energy harvesting from low frequency applications using piezoelectric materials. *Applied Physics Reviews*, 1(4), 041301.
 - [8] Yang, Z., & Zu, J. (2016). Toward harvesting vibration energy from multiple directions by a nonlinear compressive-mode piezoelectric transducer. *IEEE/ASME Transactions on Mechatronics*, 21(3), 1787-1791.
 - [9] Yang, Z., & Zu, J. (2016). Comparison of PZN-PT, PMN-PT single crystals and PZT ceramic for vibration energy harvesting. *Energy Conversion and Management*, 122, 321-329.
 - [10] Fan, F. R., Tian, Z. Q., & Wang, Z. L. (2012). Flexible triboelectric generator. *Nano Energy*, 1(2), 328-334.
 - [11] Niu, S., & Wang, Z. L. (2015). Theoretical systems of triboelectric nanogenerators. *Nano Energy*, 14, 161-192.
 - [12] Balakrishna, A. R., & Huber, J. E. (2016). Nanoscale domain patterns and a concept for an energy harvester. *Smart Materials and Structures*, 25(10), 104001.
 - [13] Wang, D., Wang, L., & Melnik, R. N. Vibration energy harvesting based on stress-induced polarization switching: a phase field approach, submitted, 2017.
 - [14] Pertsev, N. A., Zembilgotov, A. G., & Tagantsev, A. K. (1998). Effect of mechanical boundary conditions on phase diagrams of epitaxial ferroelectric thin films. *Physical review letters*, 80(9), 1988.
 - [15] Wang, J., & Kamlah, M. (2009). Three-dimensional finite element modeling of polarization switching in a ferroelectric single domain with an impermeable notch. *Smart Materials and Structures*, 18(10), 104008.
 - [16] Van Lich, L., Shimada, T., Nagano, K., Hongjun, Y., Wang, J., Huang, K., & Kitamura, T. (2015). Anomalous toughening in nanoscale ferroelectrics with polarization vortices. *Acta Materialia*, 88, 147-155.3341.
 - [17] Comsol multiphysics finite element analysis software. <http://www.comsol.com>.

**8th ECCOMAS Thematic Conference on Smart
Structures and Materials**

**6th International Conference on Smart Materials
and Nanotechnology in Engineering**

SMART 2017

5 – 8 June 2017, Madrid, Spain

Alfredo Güemes, Ayech Benjeddou, José Rodellar and Jinsong Leng (Eds)



**8th Conference on
Smart Structures and Materials
SMART 2017**

**6th International Conference on
Smart Materials and Nanotechnology
in Engineering
SMN2017**

**5 – 8 June 2017
Madrid, Spain**

A publication of:

**International Center for Numerical
Methods in Engineering (CIMNE)**
Barcelona, Spain



Printed by: Artes Gráficas Torres S.L., Huelva 9, 08940 Cornellà de Llobregat,
Spain

ISBN: 978-84-946909-3-8

Fibre Optic Sensor Embedding in Metals using Low Cost TIG Welding and High Precision Laser Braze	577
<i>T. Grandal, S. Fraga, G. Castro, E. Vazquez, J. A. Vazquez and A. Zornoza</i>	
Implementation of FBG Optical Sensors within a Laser-Assisted Fiber Placement Process for On-Line Monitoring of High Temperature Thermoplastic Materials Consolidation	583
<i>D. Saenz-Castillo, F. Rodriguez-Lence and A. Güemes</i>	
Laminates with Integrated Piezoelectric Transducers: Influence of the Transducers Location along the Thickness-axis on the Structural Performance	594
<i>X. Chen, Y. Meyer, R. Lachat and M. Ouisse</i>	
Registration of Technological Strain in Polymer Composite Samples using Embedded Fiber - Optic Strain Sensors	606
<i>V.P. Matveenko, N.A. Kosheleva, I.N. Shardakov and A.A. Voronkov</i>	
 Energy Harvesting, Power and Storage	
An Asymptotically Correct Beam Type Piezoelectric Energy Harvester Model	618
<i>S. Banerjee and S. Roy</i>	
Development of Li_{1.4}Al_{0.4}Ti_{1.6}(PO₄)₃ Solid Electrolyte-Based Power Composites: Characterisation of Electrical Properties and Mechanical Properties	619
<i>G. Liao, S. Geier, T. Mahrholz, P. Wierach and M. Wiedemann</i>	
Experimental Validation of a Porous Piezoelectric Energy Harvester	630
<i>G. Martinez-Ayuso, H.H. Khodaparast, Y. Zhang, C.R. Bowen, M.I. Friswell, A.D. Shaw, H. Madinei and J.I. Roscow</i>	
Flywheel Proof Mass Transducer for Energy Harvesting Applications	642
<i>A. Kras and P. Gardonio</i>	
Investigation of Interfacial Conditions for Li_{1.4}Al_{0.4}Ti_{1.6}(PO₄)₃ Solid Electrolyte-based Multifunctional Energy Storage Devices	654
<i>G. Liao, S. Geier, T. Mahrholz, P. Wierach and M. Wiedemann</i>	
Phase-Field Study of Stress-Induced Polarization Switching for Vibration Energy Harvesting	666
<i>D. Wang, R. Melnik and L. Wang</i>	
Preliminary Investigation of the Energy Harvesting System Intended for use on an ORC Microturbine	674
<i>T. Z. Kaczmarczyk, G. Żywica, E. Ihnatowicz, M. Lubieniecki and J. Roemer</i>	
Vibration Energy Harvesting with Electromagnetic and Piezoelectric Seismic Transducers: Experimental Results	686
<i>L. Dal Bo and P. Gardonio</i>	

